ELSEVIER

Contents lists available at ScienceDirect

Geomorphology

journal homepage: www.journals.elsevier.com/geomorphology



A pre-Pliocene origin of the glacial trimline in the Ellsworth Mountains and the prevalence of old landscapes at high elevations in West Antarctica

David Small^{a,*}, Michael J. Bentley^a, Stewart P.H.T. Freeman^b, Angel Rodés^{c,1}, Sheng Xu^{b,2}

- a Department of Geography, Durham University, Durham DH1 3LE, UK
- ^b Scottish Universities Environmental Research Centre, East Kilbride G75 0QF, UK
- ^c NERC NEIF-CN (formerly CIAF), Scottish Universities Environmental Research Centre, East Kilbride G75 0QF, UK

ARTICLE INFO

Kevwords:

West Antarctic Ice Sheet Cosmogenic nuclides Glacial trimline Ellsworth Mountains

ABSTRACT

A glacial trimline at high elevations in West Antarctica informs on previous warm-based glaciation that occurred during an earlier stage of Antarctic Ice Sheet evolution. A multi-million-year history of theses landscapes has previously been evidenced in a few disparate locations. Here we present new cosmogenic nuclide analyses (¹⁰Be and ²⁶Al) from a total of 60 samples (clasts and bedrock) at high elevations in several hard-to-access locations across the interior of West Antarctica. In the Sentinel Range of the Ellsworth Mountains this trimline occurs at the highest elevations of any sites in West Antarctica (~3000 m asl). These new data reveal that clasts and bedrock, both above and below the trimline, have long exposure histories with minimum exposure-burial histories of 0.9-2.6 Ma. Accounting for low rates of erosion extends these exposure-burial histories to 2.7-4.8 Ma. Under the assumption of cyclical exposure-burial for proportions of glacial-interglacial cycles we show that some of our samples have exposure-burial histories extending back to the Miocene. We also present new data from the nearby Heritage Range where our new data supports previous work potentially extends the inferred persistence of the location of the West Antarctic ice sheet divide to >2.1 Ma. Finally, we present new data from two isolated nunataks (Mount Woollard and Mount Johns) located deep in the interior of the West Antarctic Ice Sheet near the main ice divide. Paired nuclide analyses of samples from these nunataks also shows long exposure histories and unambiguous evidence of past burial within the last ~100 ka. Such a thickening is not currently represented in ice-sheet models.

1. Introduction

Understanding the long-term evolution of the West Antarctic Ice Sheet (WAIS) can shed light on its propensity for collapse and aids predictions of its future evolution (e.g. Naish et al., 2009; Pollard and DeConto, 2009; Hein et al., 2016). Additionally, Antarctica - including West Antarctica - contains rare terrestrial records of ice-sheet response to global climate change over longer time periods, specifically since the Miocene and Pliocene (De Schepper et al., 2014; Gasson et al., 2016; Levy et al., 2016). Given that these periods are considered potential analogues for a future warm, high carbon dioxide world understanding the concomitant evolution of the ice sheets and global climate during these times is a recognised research priority (e.g., Blasco et al., 2024; Halberstadt et al., 2024; Haywood et al., 2024).

Geochronological evidence, specifically from terrestrial cosmogenic nuclides, provides important constraints on the processes and timings of past ice-sheet changes. However, in Antarctica its interpretation is often complicated by the fact that ubiquitous low erosion rates (Marrero et al., 2018) and repeated waxing and waning of the ice sheet (Naish et al., 2009) have preserved relict landscape(s) where cosmogenic nuclide inventories often reflect long and complex exposure-burial histories. Analysis of multiple nuclides with differing half-lives, in this case ¹⁰Be (1.39 Ma) and ²⁶Al (0.72 Ma), can allow these complex exposure-burial histories to be investigated and, under various assumptions, provide minimum constraint on the total history experience by a given sample. Combining these constraints with other lines of evidence allows inferences about long term ice sheet histories to be made (e.g. Hein et al., 2016; Jones et al., 2017; Sugden et al., 2017; Spector et al., 2020).

E-mail address: david.p.small@durham.ac.uk (D. Small).

^{*} Corresponding author.

¹ Now at: Department of Geography, Universidade de Santiago de Compostela, Spain.

² Now at: School of Earth System Science, Tianjin University, Tianjin 300072, China.

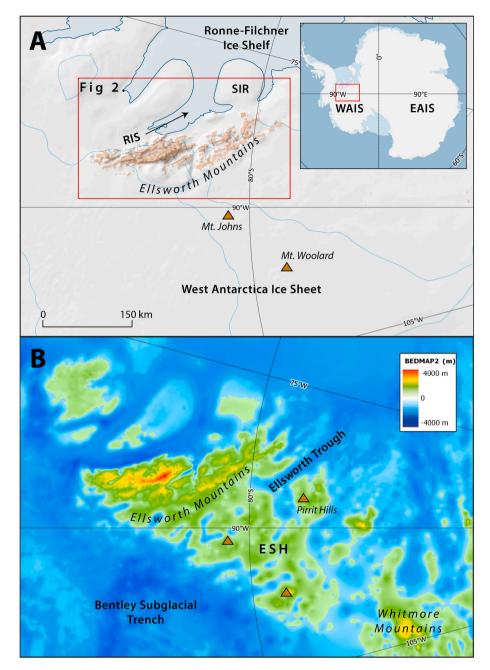


Fig. 1. A) Location map of Ellsworth Mountains showing place names mentioned in text. Black box delimits Fig. 2. B) Bed topography from BEDMAP2 (Fretwell et al., 2013) showing main subglacial features mentioned in the text. Inset shows location of both panels in Antarctica. WAIS = West Antarctic Ice Sheet, EAIS = East Antarctic Ice Sheet, RIS = Rutford Ice Stream, SIR = Skytrain Ice Rise, ESH = Ellsworth Subglacial Highlands. Base imagery is from Quantarctica GIS package (Matsuoka et al., 2021) compiled by the Norwegian Polar Institute (http://www.quantarctica.org/).

Recent studies have indicated that exposed areas across large parts of the WAIS have potential to record long, multi-million-year histories of ice sheet change (Hein et al., 2016; Sugden et al., 2017; Spector et al., 2020; Small et al., 2021). In this paper we present data from the Sentinel Range of the Ellsworth Mountains and nunataks rising from their subglacial extension (the Ellsworth Subglacial Highlands) in the interior of the WAIS to investigate the long-term history of the central part of the ice sheet.

We present cosmogenic nuclide results from glacial erratics and bedrock in the Sentinel Range to investigate the age of a glacial trimline in this sector of the Ellsworth Mountains. Paired nuclide analyses ($^{10}{\rm Be},^{26}{\rm Al}$) are modelled to establish minimum exposure histories and to test the length of cyclical exposure-burial scenarios that could produce the measured concentrations and ratios. Further data from the Heritage

Range and nunataks within the WAIS interior are modelled using the same approach. The modelled histories of data from the Heritage Range are related to the longer-term position of the WAIS ice divide. The data from the interior WAIS sites has potential to inform on any thickening of the ice divide during previous periods of ice sheet change.

2. The glacial trimline in the Ellsworth Mountains

The Ellsworth Mountains, the highest mountains in Antarctica, span c. 350 km North-South and c. 80 km East-West along the landward margin of the Ronne Ice Shelf (Fig. 1A). The Ellsworths can be separated into two distinct groups; the higher, alpine Sentinel Range to the North are separated by the Minnesota Glacier from the lower Heritage Range to the South (Fig. 2). The Sentinel Range commonly exceeds 3500 m asl

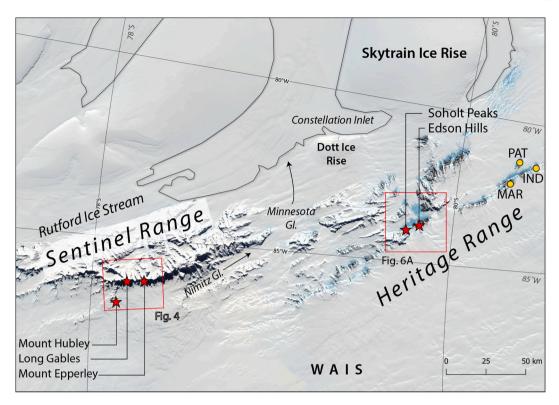


Fig. 2. Landsat true colour image of Ellsworth Mountains showing sample sites presented in this study (red stars) and samples sites of Hein et al. (2016) (yellow circles). MH = Mount Hubley, LG = Long Gables, ME = Mount Epperley, SP = Soholt Peaks, EH = Edson Hills, MAR = Marble Hills, PAT = Patriot Hills, IND = Independence Hills, DIF = Drake Ice Fall. Black line is present day grounding line (Bindschadler et al., 2011). Base Imagery is from Landsat image mosaic of Antarctica (Bindschadler et al., 2008).

and forms a prominent west-facing escarpment that acts as a barrier preventing direct west-east flow of ice from the main WAIS into the Ronne Ice Shelf. The Heritage Range contains few peaks over 2000 m and is characterised by a series of NNW-SSE trending ridges that display alpine morphology but are now, in many places, subsumed or transgressed by the main WAIS. Katabatic winds sweep down from the WAIS divide and cross the Heritage Range, producing large blue ice areas on lee sides of escarpments (Denton et al., 1992; Fogwill et al., 2012; Woodward et al., 2022). The Ellsworth Subglacial Highlands are an extension of the Ellsworth Mountains that continue for ~300 km to the south and west (Fig. 1B). These subglacial highlands are hypothesised to have been a nucleation area of the WAIS (Bentley et al., 1960) and exhibit alpine-like topography dissected by deep glacially excavated troughs (Ross et al., 2014; Napoleoni et al., 2020). The Ellsworth Subglacial Highlands are predominantly <1000 m asl with a few higher nunataks protruding above the WAIS surface, such as at Mount Woollard, Mount Johns, and the Pirrit Hills (Fig. 1).

Glacial geomorphological mapping documents a distinct erosional trimline throughout the Ellsworth Mountains (Denton et al., 1992). On their western side this trimline is \sim 400–650 m above the present ice surface with an elevation gradient that reflects the present-day ice sheet surface (Denton et al., 1992; Ross et al., 2014). This regionally consistent pattern of trimline elevations led Denton et al. (1992) to argue that the trimline represents an upper ice sheet surface rather than an englacial thermal boundary which is a more common interpretation of such features, particularly in the northern hemisphere (cf. Kleman and Stroeven, 1997; Fabel et al., 2012; McCarroll, 2016). In the Sentinel Range ridges above the trimline are characterised by numerous rock pinnacles and are highly serrated (Fig. 3B/C), erratics are absent, and there is no evidence of glacial erosion (Denton et al., 1992). Below the trimline pinnacles are absent from ridges and there is evidence of glacial erosion in the form of ice-moulded bedrock and striations. Additionally, small patches of till and glacially transported clasts and boulders are observed (Denton et al.,

1992). In the Heritage Range the trimline is discontinuous and is only observed on the highest peaks and ridges. A second, lower weathering limit in the Heritage Range at elevations ~200–475 m above modern ice is interpreted as representing the maximum extent of glacial expansion during the Last Glacial Maximum (LGM) (Bentley et al., 2010).

The presence of ice-moulded bedrock and striations below the Ellsworth trimline is consistent with erosion under warm-based ice near the upper margins of a formerly expanded WAIS (Denton et al., 1992; Sugden et al., 2017). Under present conditions the presence of coldbased ice in the Ellsworth Mountains is ubiquitous and the existence of warm-based ice would require temperatures significantly warmer than present (cf. Casassa et al., 2004). Sugden et al. (2017) investigated the age of the upper trimline at sites in the Heritage Range (Fig. 2) by analysing multiple cosmogenic nuclides (¹⁰Be, ²⁶Al, ²¹Ne) in glacial erratics and a bedrock core. They show that some glacially transported clasts have exposure histories >1.4 Ma and perhaps as much as 3.5 Ma. Modelling of the nuclide concentrations within their bedrock core reveals a minimum exposure history of 3.5-5.1 Ma. Under the assumption that it was formed by warm-based ice, Sugden et al. (2017) argue that these exposure histories are consistent with the upper trimline being millions of years old and propose that it was formed prior to the distinct cooling of the mid-Miocene at 14 Ma and the concomitant expansion of the WAIS (cf. Shevenell et al., 2004; Warny et al., 2009). A similar scenario is proposed by Spector et al. (2020) based on bedrock samples from nunatak groups in the interior of the WAIS, including the Pirrit Hills. Samples from high elevations where there is no evidence of former ice cover have exceptionally long exposure histories (> 10 Ma).

Existing exposure ages from the Heritage Range show a general decline in exposure age and increase in burial history with decreasing elevation (Hein et al., 2016). This trend is consistent with an overall lowering of the average ice surface with respect to the exposed uplands (Hein et al., 2016; Sugden et al., 2017). It is inferred that this lowering is related to progressive excavation of the major subglacial troughs

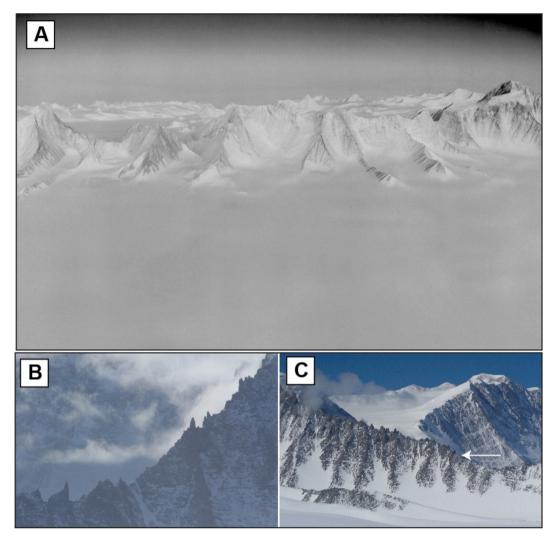


Fig. 3. A) Oblique aerial photograph (TMA 565–122–14/12/1959) showing the main west facing escarpment of the Sentinel Range with cirques hosting local glaciers that are confluent with main ice sheet. Mount Epperley is the highest peak at right hand edge of image. Image has been edited to improve contrast. B) Photograph of typical ridge morphology above the Ellsworth trimline, note the delicate rocky pinnacles. C) Photograph of transition from serrated and pinnacled ridge to smoother ridge morphology at Ellsworth trimline. Approximate location of transition shown by white arrow.

 Table 1

 Summary site location information for sample sites presented here.

Site	Latitude	Longitude	Elevati (m)	Elevation range (m)		Measurements	
Sentinel Range			Мах	Min	Ве	Be + Al	
Long Gables	-78.23	-86.29	2825	2334	12*	9	
Mount Epperley	-78.43	-86.03	2930	2547	15	2	
Mount Hubley	-78.14	-86.68	2335	2250	6	4	
Heritage Range							
Sohalt Peaks	-79.73	-83.98	1330	958	9	4	
Edson Hills	-79.78	-83.81	1247	988	6	-	
Interior WAIS sites							
Pirrit Hills	-81.13	-85.55	1730	1684	2	_	
Mount Woolard	-80.54	-96.68	2467	2388	6	2	
Mount Johns	-79.63	-91.27	2192		3	2	
* One sample (LOI	N-11-MJB) is	Al only					

surrounding the Heritage Range (Hein et al., 2016) with implications for the age of subglacial lakes such as Lake Ellsworth (Siegert et al., 2004) and the records they potentially contain. Additionally, knowing the age of the trimline provides constraints on models of long-term Antarctic Ice Sheet history (cf. Golledge et al., 2013). There is compelling evidence that the trimline in the Heritage Range, and a potential extension of it in the Pirrit Hills, is millions of years old and that it possibly dates to the Miocene (Sugden et al., 2017; Spector et al., 2020). Given consistent regional trends in trimline elevation it is reasonable to suggest that the trimline in the Sentinel Range is of a similar age, but this assumption remains untested.

3. Sample settings

3.1. Sentinel Range

Samples were collected during the austral summer of 2005/2006 from three sites in the Sentinel Range: Long Gables, Mount Epperley, and Mount Hubley (Table 1). This sampling was part of a wider study that aimed to constrain WAIS evolution since the Last Glacial Maximum (LGM) (cf. Bentley et al., 2010) thus most samples were taken from glacially transported clasts and boulders as these were considered more likely to record the most recent surface elevation changes. The sample sites are located close to the present-day ice divide that separates ice flowing south into the Nimitz Glacier from ice flowing north into the upstream catchment of the Rutford Ice Stream.

The samples from Long Gables and Mount Epperley were collected

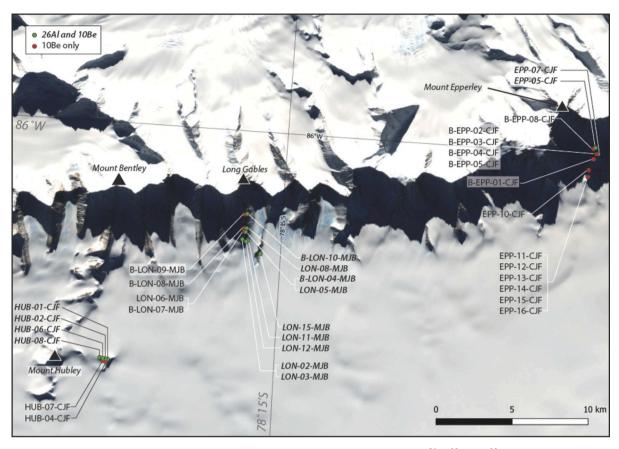


Fig. 4. Location map of Sentinel Range sample sites showing locations of all TCN samples analysed for paired ²⁶Al/¹⁰Be and ¹⁰Be only. Base Imagery is from Landsat image mosaic of Antarctica (Bindschadler et al., 2008).

from vertical transects on spurs that extend west from the main escarpment and bound deep cirques that host locally sourced ice (Fig. 3 and Fig. 4). These transects extend from near the present-day ice surface (2250 m asl) up to the approximate elevation of the glacial trimline. Given the glaciological setting and the consistent quartzite lithology of the Sentinel Range (Webers and Sporli, 1983) true erratic lithologies were not observed but samples were preferentially collected from quartzite boulders and clasts that were visually distinct from the nearby bedrock and were in locations consistent with glacial transport (Fig. 5A-C). Below the trimline bedrock samples were collected from outcrops showing evidence of glacial modification. Above the trimline bedrock samples were collected from the top of bedrock pinnacles (Fig. 5D) and the crests of prominent ridges. Given the regional flow patterns the glacially transported clasts along the west side of the Sentinels are most likely to be locally sourced and thus were potentially delivered as supraglacial material from higher elevations prior to deposition (the main escarpment exceeds 3500 m asl at these locations). The distribution of exposure ages at these sites is therefore likely the product of local thickening(s) of cirque glaciers in concert with expansion of the WAIS (cf. Denton et al., 1992). Under the assumption that the trimline was formed by wet-based glaciation (Sugden et al., 2017) it can be hypothesised that exposure histories of glacially transported material below the trimline post-date its formation since a dynamic wet-based ice sheet would have likely removed pre-trimline material.

Mount Hubley has a different glaciological setting. It is an isolated nunatak that lies $\sim\!13$ km west of the main Sentinel escarpment and ~5 km west of the long spur that extends west from Mount Bentley (Fig. 4). Mount Hubley is $\sim\!2650$ m asl and stands $\sim\!500$ m above the local ice surface at 2140 m asl. Samples were collected from a vertical transect 110–195 m above present-day ice on a small outlying nunatak west of Mount Hubley. Striations near Mount Hubley trend north-south and

record the deflection of ice flowing west from the Sentinel cirques by the main WAIS and towards the upper reaches of the Rutford Ice Stream (Denton et al., 1992). The lack of far-travelled erratics and its relative proximity to the Sentinel Range suggest that glacially-transported clasts on Mount Hubley were deposited by thicker ice that flowed from the west facing cirques of the Sentinel Range. These clasts may have previously been exposed at higher altitudes prior to deposition on Mount Hubley.

3.2. Heritage Range

The sites in the Heritage Range were also sampled during the austral summer of 2005/2006 with the aim of constraining post-LGM thinning (cf. Bentley et al., 2010). The two sites (Soholt Peaks and Edson Hills; Table 1) are located on the north and south sides of the Drake Icefall respectively (Fig. 6). This icefall is ~3 km wide and is one of several locations where the WAIS flows through the topographic barrier of the Heritage Range. The Drake Icefall feeds into Union Glacier at its junction with Schanz Glacier; from here it flows east to join the lower Rutford Ice Stream at Constellation Inlet (Fig. 2). On the down-ice (east) sides of both the Soholt Peaks and Edson Hills are extensive blue ice areas with associated blue ice moraines (Fig. 6) (Fogwill et al., 2012). In blue ice areas ice flow adjusts to compensate for losses due to ablation bringing deeper, blue ice to the surface along with any debris contained within the ice (Fogwill et al., 2012; Hein et al., 2016). Due to compressional flow at right angles to the main glacier flow direction the debris forms extensive active deposits at the ice margin (Fogwill et al., 2012; Westoby et al., 2016). These can be deposited as relict moraines during episodes of ice surface lowering if material is not removed by lateral flow (Fogwill et al., 2012). On higher slopes, series of nested lateral moraines trend north-south, parallel to the current ice margin, and record past changes



Fig. 5. Example sample photographs from A-D: Sentinel Range. *E-*F: Heritage Range, in panel E white arrow denotes sampled clast, note the distinct moraine ridge on which the clast sits and active blue ice moraines in middle distance. G: Pirrit Hills. H: Mount Woollard, and I) Mount Johns. (For interpretation of the references to colour in this figure legend, the reader is referred to the web version of this article.)

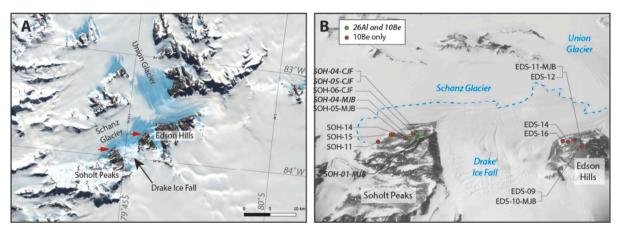


Fig. 6. A) Landsat true colour image (Bindschadler et al., 2008) of Heritage Range sample sites (Soholt Peaks and Edson Hills). Red arrows point to currently active blue ice moraines (cf. Fogwill et al., 2012). B) Oblique aerial photograph of Heritage Range sites and Drake Ice Fall (TMA 1496-193 – 14/12/1964). Sample locations and extent of main blue ice area are annotated. (For interpretation of the references to colour in this figure legend, the reader is referred to the web version of this article.)

in ice thickness (cf. Fogwill et al., 2012; Hein et al., 2016). The Heritage sites are located below the trimline reported by Denton et al. (1992) and also below the lower weathering limit reported by Bentley et al. (2010). Consequently, these glacial deposits post-date trimline formation (Sugden et al., 2017). Samples were collected from vertical transects that span 372 m and 260 m above the ice for the Soholt Peaks and Edson Hills respectively. The maximum elevations of 1200–1300 m asl are

~400 m above present-day ice. Samples were collected from glacially transported erratic clasts located on moraine crests (Fig. 5E), perched on bedrock, and located on the surface of till deposits (Fig. 5F). Exhumation from depth is unlikely given the absence of features indicating periglacial activity. Given the orientation of the moraines it can be inferred that glacial material was deposited by previously thicker ice in the Union and Schanz glaciers at time(s) in the past when the ice flow

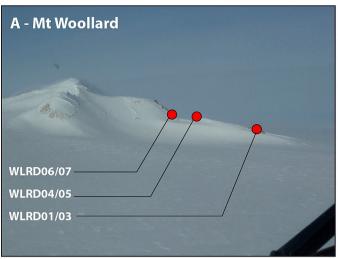




Fig. 7. A) Field photograph of Mount Woollard showing locations of sample on Northwest ridge. B) Field photograph of Northeast face of Mount Johns.

configuration was broadly like present (cf. Hein et al., 2016).

3.3. Interior WAIS sites

The Pirrit Hills are located approximately halfway between the main WAIS divide and the grounding line. They are the subaerial expression of a large high-elevation block that is separated from the Heritage Range by the Ellsworth Trough (Fig. 1B). Katabatic winds produce large blue ice areas with associated blue ice moraines on the eastern side of the Pirrit Hills. Minimally weathered glacial deposits, inferred to represent the LGM ice limit, are observed up to ~330 m above present-day ice levels (Spector et al., 2018, 2019). Associated with these fresh glacial deposits is bedrock that preserves wind polish and cavernous weathering while displaying no signs of glacial erosion. Two samples were collected in 2005/2006 from glacially transported boulders that are perched on an ice moulded bedrock ridge (Fig. 5G). South of this ridge, $350\mbox{--}400~\mbox{m}$ below the samples, is a blue ice area with blue ice moraines. To the north katabatic winds have deposited a snow ramp that slopes away from the bedrock ridge with an upper limit 50-100 m below the samples. From this it is inferred that the ice surface would need to thicken on the southern side of the ridge to deposit these boulders, potentially as relict blue ice deposits. Notably boulders of similar sizes (>20 m³) are observed on moraines close to present day ice. These samples are likely to have been deposited due to thickening of the ice centred over the Pirrit Hills massif, which would occur in concert with thickening of the ice stream feeder arms at its margins.

Mount Woollard and Mount Johns are isolated nunataks that represent high points of the Ellsworth Subglacial Highlands and are located approximately 320 and 175 km southwest of the Ellsworth Mountains respectively (Fig. 1A). Mount Woollard (2675 m asl) rises ~300 m above present-day ice level while Mount Johns (>2000 m asl) protrudes only ~100 m (Fig. 7). The nunataks are located on the main WAIS ice divide separating ice flowing into the Amundsen and Weddell seas. The high elevation blocks are bounded by deep glacially excavated troughs that feed into the Bentley Subglacial Trench to the west and are potentially connected with troughs incised into the eastern flank of the Ellsworth Subglacial Highlands (Ross et al., 2014). There is no higher topography in the vicinity of either nunatak thus it is considered unlikely that material could have been exposed at elevations higher than today. At Mount Woollard six samples were collected in 2014/2015 near the crest of the from the Northwest ridge (Fig. 7A). All samples were locally derived clasts perched on low-angle bedrock surfaces (Fig. 5H). The clasts appear to have been derived from local gneissic outcrops and are inferred to have only been moved a few metres, presumably by ice.

At Mount Johns three samples were collected from a narrow (\sim 10 m) ledge located approximately 50 m below the summit (Fig. 7B). The edges of this ledge retain striations orientated \sim 020° - 200°. Three loose blocks were collected from this ledge (Fig. 5H). Given the glaciological isolation of these nunataks the inference is that exposure histories from these nunataks will be the result of surface elevation changes of the main WAIS ice divide through time.

4. Methods

4.1. Sample preparation and analysis

Samples were collected as whole clasts, with the top surfaces marked, or taken from larger boulders by hammer and chisel. Skyline elevations were measured, and subsequent shielding corrections calculated using the online calculator (https://stoneage.ice-d.org/math/skyl ine/skyline_in.html). Sample elevations and the elevation of the local ice sheet surface were recorded by handheld GPS. Sample thicknesses were measured, and samples were subsequently crushed to 250-500 µm. Beryllium and Aluminium were extracted from clean quartz at the Cosmogenic Nuclide Laboratory of the School of GeoSciences, University of Edinburgh, and the NERC Cosmogenic Isotope Analysis Facility (CIAF) following established procedures (Kohl and Nishiizumi, 1992; Child et al., 2000). Beryllium and aluminium ratios were measured on the 5MV accelerator mass spectrometer (AMS) at the Scottish Universities Environmental Research Centre (Xu et al., 2010). AMS ratios were normalised and ¹⁰Be/⁹Be ratios background corrected for procedural blanks. The ²⁶Al/²⁷Al procedural blanks for samples processed at the University of Edinburgh during this period produced low currents thus no background correction could be made however given the high measured ratios and the low background ratios produced by blanks from subsequent ²⁶Al/²⁷Al batches the calculated concentrations are likely insensitive to this. Apparent exposure ages were calculated using version 3 of the online calculator formerly known as the CRONUS-Earth exposure age calculator (cf. Balco et al., 2008: accessed June 2021; checked January 2025) using the nuclide dependent Lifton-Sato-Dunai (LSDn) scaling scheme (Lifton et al., 2014) as the scheme better predicts production rates at high-elevation-high-latitude locations (cf. Balter-Kennedy et al., 2020). Input data are presented in Table S1.

4.2. Exposure-burial modelling

Exposure-burial scenarios were investigated using a MATLAB \odot model. The concentrations of cosmogenic nuclides (N_k) were calculated

Table 2Parameters used in two-stage forward modelling of nuclide concentrations and parameters used to define parameter spaces for cyclical exposure-burial.

Two-stage model parameters	Values	Cyclical model parameters	Values
Time increment (ka)	20	Time increment (ka)	5
Initial exposure range (ka)	0–5000	Initial exposure (Pliocene - ka)	0-3500
Burial duration (ka)	0-5000	Initial exposure (Miocene - ka)	0-15,000
Sub-aerial erosion rate (m/Ma)	0–1.5	Sub-aerial erosion rate (m/Ma)	0–1.5
Sub-glacial erosion rate (m/Ma)	0–1.5	Sub-glacial erosion rate (m/Ma)	0–1.5
Erosion rate increment (m/Ma)	0.1	Erosion rate increment (m/Ma)	0.1
Total number of combinations	16,128,256		
Iterations	2,000,000		

for exposure (eq.1) and burial (eq.2) periods following Jones et al. (2017) as follows:

$$N_{k}^{i} = N_{k}^{i-1} exp \left[-\left(\lambda_{k} + \frac{\rho \varepsilon_{sa}}{\Lambda}\right) t_{e} \right] + \frac{P_{k}}{\lambda_{k} + \frac{\rho \varepsilon_{sa}}{\Lambda}} \left(1 - exp \left[-\left(\lambda_{k} + \frac{\rho \varepsilon_{sa}}{\Lambda}\right) t_{e} \right] \right)$$

$$(1)$$

and

$$N_k^i = N_k^{i-1} exp \left[-\left(\lambda_k + \frac{\rho \varepsilon_{sg}}{\Lambda}\right) t_b \right]$$
 (2)

where P_k and λ_k are the production rate (atoms g^{-1} a⁻¹) and decay constant (s^{-1}) for nuclide k respectively. ρ is the density of the rock (g cm⁻³), ϵ_{sa} and ϵ_{sg} are sub-aerial and sub-glacial erosion rates (cm a⁻¹), Λ is the attenuation length (g cm⁻²), and t_e and t_b are the durations (a) of exposure and burial. Sample-specific production rates (spallation and muons) and attenuation lengths were calculated using MATLAB© code adapted from the CRONUScalc framework and a global production rate dataset (Borchers et al., 2016; Marrero et al., 2016; Jones et al., 2019). To model concentrations we used a production rate time-averaged over the last 14 ka. This is because variations in production rates at high latitudes are dominated by changes in solar modulation however, in the CRONUScalc framework models for this effect only extend to 14 ka so over the multi-million-year timescales that we are investigating the effect in our calculations is negligible.

We first modelled the evolution of nuclide inventories over a simple two-stage exposure burial history for a conservative range of initial exposure times, burial durations and erosion rates (Table 2). This approach essentially assumes the sample was exposed immediately prior to sampling and no nuclides have accumulated in the present period of exposure. A single period of continuous exposure with zero erosion followed by a single period of continuous burial provides the fastest scenario by which a sample can evolve to any given point on the twoisotope plot. Consequently, such scenarios provide minimum constraints of the exposure-burial of a given sample. In reality erosion rates, while low can be non-zero in Antarctica (cf. Marrero et al., 2018), thus modelling exposure-burial periods for a range of low potential erosion rates $(0-1.5 \text{ mm ka}^{-1} [0-1.5 \text{ m/Ma}], \text{ cf. Marrero et al., } 2018)$ provides a more realistic estimate of minimum histories. Model iterations that match measured concentrations and ratios for a given sample within its 2σ uncertainties were accepted. We calculated mean exposure durations, burial durations, total sample histories, and associated standard deviations from accepted scenarios from 2 million model iterations.

To provide a more conservative estimate of total exposure burial history we adapted the approach of investigating cyclical exposure-burial (Bierman et al., 1999; Balco et al., 2014; Briner et al., 2014; Jones et al., 2017; Spector et al., 2020). Samples are assumed to have been exposed for a proportion of a glacial-interglacial cycle reflecting

fluctuations in the ice sheet surface. Our model uses 40 kyr and 100 kyr cycles (40 kyr prior to 2.6 Ma, 50:50 2.6–1 Ma, 100 kyr after 1 Ma). The model was used to define two parameter spaces using ranges and values (Table 2) for total cyclical exposure-burial histories of 3.5 Ma and 15 Ma (i.e. Pliocene and Miocene).

5. Results

5.1. ¹⁰Be and ²⁶Al results

Apparent ¹⁰Be and ²⁶Al exposure ages are presented in Table 3. Single nuclide exposure ages range from 25 to 2379 ka in the Sentinel Range (Mount Hubley, Long Gables, Mount Epperley), 38-1348 ka in the Heritage Range (Soholt Peaks, Edson Hills), and 132-250 ka from the interior WAIS sites (Mount Woollard, Mount Johns, Pirrit Hills), Of the 22 samples with paired ²⁶Al and ¹⁰Be analyses nuclide concentrations range from 5.4 \times 10⁵ to 9.4 \times 10⁷ atoms g⁻¹ and 2.5 \times 10⁶ to 4.2 \times 10⁸ atoms g⁻¹ for ¹⁰Be and ²⁶Al respectively. The paired concentrations give normalised 26 Al/ 10 Be ratios $\sim 0.32-0.79$ (Fig. 8). A single sample (Fig. 8A: EPP-05-CJF) lies in the 'forbidden zone' above the steady-state erosion island. We do not consider this sample in further discussions. One sample (Fig. 8A: LON-08-MJB) overlaps with the lower limb of the steady-state erosion island, which is consistent with, but does not mandate, a single stage of exposure (cf. Mukhopadhyay et al., 2012). All the other samples display ²⁶Al/¹⁰Be ratios that plot within the zone of complex exposure implying that they have experienced at least one period of burial in the past.

5.2. Two-stage exposure burial modelling

The modelled minimum (zero-erosion) exposure-burial histories are 720-2620 ka for samples from the interior WAIS sites, 460-1200 ka for the Heritage Range, and 900-4300 ka for the Sentinel Range (Table 4 and Fig. 9). Exposure-burial histories for these sites, based on combinations of subaerial and subglacial erosion rates, are 2665-4772 ka, 748-4105, and 2561-4817 respectively (Table 4 and Fig. 9). These histories assume that the samples have been exposed and buried at the same elevation throughout their history. This assumption is valid for bedrock samples (B/LON-04-MJB, B/LON-10-MJB) but may not hold for clast/boulder samples. The interior WAIS sites (Mount Woollard and Mount Johns) have no higher topography in their vicinity thus it is unlikely that these samples could have been exposed at higher elevations in the past, However, in the Sentinel and Heritage Ranges the presence of higher topography up-ice of our sample sites means samples could have previously been exposed at higher elevations, with higher production rates, than their current locations. Similarly at all sites samples could potentially have been exposed at lower elevation during times of reduced WAIS ice volume (cf. Naish et al., 2009) and subsequently been remobilised and deposited at their current locations. To test the sensitivity of our results to elevation changes we modelled minimum histories assuming elevations 500 m lower (all sites) and 500 m higher (Sentinel and Heritage sites). The differences are relatively minor (Table 5) and do not influence our overall interpretation.

5.3. Cyclical exposure burial modelling

Previous work investigating long-term exposure burial histories of samples in the Transantarctic Mountains (Jones et al., 2017) assumed that samples were ice-covered for 0–100 % of a glacial-interglacial cycle with the percentage depending on the elevation of the sample above the modern ice surface (i.e. higher samples will have lower percentages). This is easy to justify when dealing with bedrock samples however most of our samples are clasts with higher potential for remobilisation. Consequently, we simplify the approach and define a parameter space for assumed cyclical exposure-burial histories over the Pliocene (3.5 Ma) and Miocene (15 Ma). Most of our samples plot towards the lower end of

Table 3
Apparent exposure ages from the Sentinel Range, Heritage Range, Pirit Hills, Mount Woollard and Mount Johns. Calculated using version 3 of the online calculator (Balco et al., 2008).

Sample	Site	Latitude (DD)	Longitude (DD)	Elevation (m)	Height above ice (m)	10 Be age (ka)	1 Sigma (internal)	1 Sigma (external)	26 Al Age (ka)	1 Sigma (internal)	1 Sigma (external)
Sentinel Range											
B-LON-04- MJB	Long Gables	-78.2292	-86.2936	2492	242	252,000	5500	16,800	181,700	3300	17,400
B-LON-07- MJB	Long Gables	-78.2292	-86.2936	2571	321	1,365,300	18,900	117,100	-	-	-
B-LON-08- MJB	Long Gables	-78.2296	-86.2834	2610	360	1,805,900	33,600	176,300	-	-	-
B-LON-09- MJB	Long Gables	-78.2290	-86.2546	2818	568	2,379,500	46,900	273,700	-	-	-
B-LON-10- MJB	Long Gables	-78.2289	-86.2540	2825	575	2,300,000	85,100	268,400	1,139,300	20,200	181,800
LON-02- MJB	Long Gables	-78.2281	-86.3105	2490	240	180,200	5000	12,200	103,800	2600	9800
LON-03- MJB	Long Gables	-78.2281	-86.3104	2488	238	149,100	3700	9800	87,400	1800	8000
LON-05- MJB	Long Gables	-78.2292	-86.2937	2565	315	433,000	9300	30,000	223,500	4400	21,900
LON-06- MJB	Long Gables	-78.2292	-86.2937	2565	315	506,500	6200	34,600	-	-	-
LON-08- MJB	Long Gables	-78.2296	-86.2834	2610	360	687,100	16,800	51,200	614,100	15,700	74,200
LON-11- MJB	Long Gables	-78.2300	-86.3117	2395	145	-	-	-	100,900	1800	9300
LON-12-	Long Gables	-78.2299	-86.3120	2395	145	304,700	7000	20,600	155,600	3200	14,800
MJB LON-15-	Long	-78.2373	-86.3394	2334	84	184,900	4000	12,100	60,400	900	5400
MJB B-EPP-01-	Gables Mt	-78.4309	-86.0085	2791	541	926,300	12,500	70,600	-	_	-
CJF B-EPP-02-	Epperley Mt	-78.4327	-86.0001	2908	658	909,300	12,200	69,000	-	-	-
CJF B-EPP-03-	Epperley Mt	-78.4329	-85.9988	2929	679	1,595,600	22,700	145,800	-	-	-
CJF B-EPP-04-	Epperley Mt	-78.4328	-85.9979	2930	680	1,793,700	25,500	173,200	-	_	-
CJF B-EPP-06-	Epperley Mt	-78.4326	-85.9957	2903	653	2,376,100	42,500	272,300		-	-
CJF B-EPP-08-	Epperley Mt	-78.4317	-85.9884	2908	658	1,456,000	19,300	127,800	-	_	-
CJF EPP-05-CJF	Epperley Mt	-78.4327	-85.9968	2906	656	2,506,700	58,800	300,900	4,566,000	1,427,200	7,827,700
EPP-07-CJF	Epperley Mt	-78.4316	-85.9877	2865	615	1,177,800	26,000	98,100	684,800	15,400	85,400
EPP-10-CJF	Epperley Mt	-78.4280	-86.0416	2640	390	706,900	11,800	51,400	_	-	-
EPP-11-CJF	Epperley Mt	-78.4281	-86.0586	2615	365	346,700	5100	22,900	_	-	-
EPP-12-CJF	Epperley Mt	-78.4281	-86.0586	2615	365	499,700	7400	34,300	_	-	-
EPP-13-CJF	Epperley Mt	-78.4282	-86.0648	2594	344	88,600	1000	5400	-	_	-
EPP-14-CJF	Epperley Mt	-78.4282	-86.0648	2594	344	430,000	7800	29,400	-	_	-
EPP-15-CJF	Epperley Mt	-78.4276	-86.0690	2547	297	70,000	1200	4400	_	-	_
EPP-16-CJF	Epperley Mt	-78.4276	-86.0690	2547	297	49,100	1000	3100	_	_	-
HUB01CJF	Epperley Mt	-78.1522	-86.6830	2335	195	142,600	2100	9000	86,000	2100	8000
HUB-02-	Hubley Mt	-78.1517	-86.6824	2335	195	138,200	3400	9100	71,800	1600	6600
CJF HUB04CJF	Hubley Mt	-78.1512	-86.6820	2302	162	25,100	600	1600	_	_	-
HUB-06-	Hubley Mt	-78.1506	-86.6815	2275	135	29,000	800	1900	16,500	400	1500
CJF HUB07CJF	Hubley Mt	-78.1054	-86.6812	2270	130	28,100	800	1900	_	_	_
HUB-08-	Hubley Mt	-78.1497	-86.6805	2250	110	52,200	1300	3400	23,500	600	2100
CJF	Hubley										

Heritage Range

(continued on next page)

Table 3 (continued)

Sample	Site	Latitude (DD)	Longitude (DD)	Elevation (m)	Height above ice (m)	10 Be age (ka)	1 Sigma (internal)	1 Sigma (external)	26 Al Age (ka)	1 Sigma (internal)	1 Sigma (external)
SOH-01-	Sohalt	-79.7347	-83.9802	1330	390	321,500	9100	22,500	204,700	4400	20,000
MJB SOH-04- CJF	Peaks Sohalt Peaks	-79.7305	-83.9541	984	44	491,700	13,600	35,600	228,500	5000	22,600
SOH-04- MJB	Sohalt Peaks	-79.7298	-83.9821	1150	210	94,600	2500	6300	78,500	1400	7200
SOH05	Sohalt Peaks	-79.7289	-83.9822	1121	181	61,100	1500	4000	-	-	-
SOH-05- CJF	Sohalt Peaks	-79.7301	-83.9551	981	41	38,000	2500	3300	27,500	500	2500
SOH06CJF	Sohalt Peaks	-79.7298	-83.9564	972	390	202,400	5200	13,600	-	-	-
SOH11	Sohalt Peaks	-79.7229	-84.0146	958	18	55,500	1400	3600	-	-	-
SOH14	Sohalt Peaks	-79.7253	-83.9844	1058	118	236,100	4300	15,400	-	-	-
SOH15	Sohalt Peaks	-79.7242	-83.9858	1019	79	103,900	1500	6500	-	-	-
EDS09	Edson Hills	-79.7795	-83.8159	1246	398	128,100	3700	8600	-	-	-
EDS-10- MJB	Edson Hills	-79.7794	-83.8157	1247	397	72,600	1400	4600	-	-	-
EDS-11- MJB	Edson Hills	-79.7778	-83.8007	1139	289	125,000	2200	7900	-	-	-
EDS12	Edson Hills	-79.7778	-83.8007	1139	289	84,100	2400	5600	-	-	-
EDS14	Edson Hills	-79.7762	-83.8058	1005	155	186,200	4900	12,500	-	-	-
EDS16	Edson Hills	-79.7741	-83.8044	988	138	95,800	2800	6400	-	-	-
WAIS Interior											
PIR05	Pirrit Hills	-81.1282	-85.5537	1684	-	1,348,200	20,500	115,400	-	-	-
PIR06	Pirrit Hills	-81.1282	-85.5537	1730	-	717,100	8700	51,600	-	-	-
WLRD01	Mt Woollard	-80.5403	-96.6876	2395	195	213,800	3800	13,800	69,600	2300	6600
WLRD03	Mt Woollard	-80.5404	-96.6872	2388	188	250,100	4900	16,500	-	-	-
WLRD04	Mt Woollard	-80.5450	-96.6803	2467	267	203,700	3100	13,000	155,800	4600	15,200
WLRD05	Mt Woollard	-80.5450	-96.6803	2467	267	180,400	1800	11,300	-	-	-
WLRD06	Mt Woollard	-80.5444	-96.6801	2431	231	201,100	3500	13,000	-	-	-
WLRD07	Mt Woollard	-80.5444	-96.6800	2429	229	160,000	2300	10,100	-	-	-
MTJN01 MTJN02	Mt Johns Mt Johns	-79.6269 -79.6269	-91.2741 -91.2741	2192 2192	100 100	152,200 132,100	1800 2200	9500 8400	89,700 -	2600 -	8500 -
MTJN03	Mt Johns	-79.6269	-91.2741	2192	100	132,000	1500	8200	79,900	2000	7400

the Pliocene parameter space or outside it completely. Of these 'outside' samples four overlap with the Miocene parameter space (Fig. 10). The remainder, with the lowest $^{26}\mathrm{Al}/^{10}\mathrm{Be}$ ratios, plot outside both parameter spaces indicating that they are not consistent with cyclical exposure-burial histories.

6. Interpretation and discussion

6.1. Sentinel Range and the age of the trimline

The ¹⁰Be apparent exposure ages of glacially transported clasts in the Sentinel Range show a general trend of decreasing age at progressively lower elevations (Fig. 11A). Erratic samples in the Sentinel Range also

exhibit evidence of increased burial with decreasing altitude (Fig. 11B). These trends can be inferred to relate to an WAIS that has fluctuated in thickness but whose overall elevation has decreased through time (Hein et al., 2016; Sugden et al., 2017; Spector et al., 2020). This overall lowering is potentially related to progressive excavation of troughs bounding the western part of the Sentinel Range (cf. Hein et al., 2016). Notably, the generally consistent trends are *not* what would be expected if samples were being pervasively remobilised to higher and/or lower elevations during repeated ice thickness fluctuations as this would produce a more random scatter of both exposure ages and burial durations. This is consistent with subsequent expansions of the ice sheet being cold based with very limited erosion and transportation of material. The apparent exposure ages presented here imply that cold-based

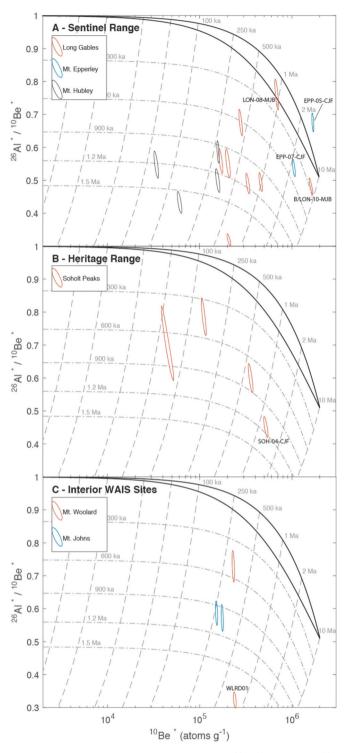


Fig. 8. Two-isotope (banana) plots of normalised (*) ²⁶Al/¹⁰Be ratios and ¹⁰Be concentrations for samples with paired ²⁶Al/¹⁰Be analyses from A) Sentinel Range, B) Heritage Range, and C) Interior WAIS sites (Mount Woollard Mount Johns). Ratios and concentrations are normalised to sample specific production rates (Table 4). Only samples mentioned specifically in the text are labelled for clarity.

ice of fluctuating thickness has been a pervasive feature in the Sentinel Range since at least c. 0.7 Ma, the oldest apparent 10 Be exposure age of a glacially transported clast sample (EPP-10-CJF). A long, million-year, history of the landscape below the trimline is also reflected in the apparent exposure ages of >1 Ma from bedrock samples below the trimline and modelled minimum exposure histories of glacially

transported clasts in the Sentinel Range (Fig. 9). Individual samples have mean minimum exposure histories of \sim 2–5 Ma with absolute minimum histories of 0.9–2.7 Ma (Table 4).

Seven samples, not including EPP-05-CJF which yielded a physically implausible ²⁶Al/¹⁰Be ratio, were located close to the mapped elevation of the Ellsworth trimline and it is inferred from the presence of delicate rock pinnacles that these samples are above the trimline. Two samples (B/LON-10-MJB, EPP-07-CJF) have paired ²⁶Al and ¹⁰Be measurements which plot below the steady state erosion island (Fig. 8A). At face value this implies that they have experienced burial at some point in their history; if cold based ice extended above the trimline it could potentially preserve pinnacles and impart a burial signal. However, there is no evidence that an ice surface has ever been higher than the trimline (Denton et al., 1992) and as argued by Sugden et al. (2017) an englacial thermal boundary origin does explain the remarkably consistent pattern of trimline elevations in the rough terrain of the Ellsworth Mountains. To reconcile these samples with the evidence that the trimline marks an absolute limit of the past elevation of ice cover requires that the samples shift to the right and/or up on the two-isotope plot (Fig. 8A). It has been noted that other high elevation sites in Antarctica where ice cover is inferred to be very unlikely display ²⁶Al/¹⁰Be ratios that are lower than expected for saturation (Spector et al., 2020). This has led to the suggestion that the ²⁶Al half-life may be shorter (~3-5 %) than the currently accepted value and/or the ²⁶Al/¹⁰Be ratio at high elevations in Antarctica may be slightly lower (<10 %) than the current scaling schemes predict (Halsted et al., 2021; also see blog by Dr. Greg Balco (February 2019): https://cosmognosis.wordpress.com/2019/02/05/st one-2000-revisited/). However, it is important to stress that the burial signal observed in the remainder of our dataset is unambiguous and our main inferences would be unaffected by potential future refinements to scaling schemes.

Bedrock samples from above the trimline have significantly older apparent ¹⁰Be exposure ages than erratic samples from below the trimline (Fig. 11A), as would be expected if the trimline represents a former ice sheet(s) upper limit (Denton et al., 1992). Very old apparent exposure ages (2.4 Ma) from delicate rock pinnacles indicate that the landscape above the Ellsworth trimline records a multi-million-year exposure history characterised by low denudation rates (~0.2 m/Ma) consistent with observations from across Antarctica (Marrero et al., 2018). This history is of a similar, and assuming the highest concentration surfaces are saturated, likely longer duration than the landscape below the trimline which itself has an exposure-burial history of at least 0.9–2.7 Ma. These inferences agree with the conclusions of Sugden et al. (2017) that the upper trimline in the Ellsworth Mountains is millions of years old.

The presence of features indicative of warm-based ice (striations, glacially smoothed bedrock) suggests that this trimline formed under a climate considerably warmer than present. Based on modelling and paleoclimate evidence Sugden et al. (2017) argued that this was most likely the mid-Miocene (~14 Ma) however they pointed out that a younger, mid-Pliocene age could not be discounted. Our modelled twostage exposure-burial histories are consistent with a multi-million-year age for the Ellsworth trimline, and we note that for all sites a significant proportion of the overall minimum-age distribution is older than the mid-Pliocene (Fig. 10). Additionally, the assumption of a two-stage history is very likely an oversimplification of the past evolution of the WAIS which has waxed and waned over orbitally forced cycles since at least the Pliocene and, potentially, since the mid-Miocene (Grutzner et al., 2003; Naish et al., 2009; Patterson et al., 2014). The results of our cyclical exposure-burial modelling indicate that a significant proportion of our samples have been exposed since at least the Miocene (Fig. 10).

The totality of evidence from the Sentinel Range extends the inference that the trimline has a multi-million-year history to the entirety of the Ellsworth Mountains (cf. Sugden et al., 2017). Our results indicate that some erratics located below the trimline have exposure histories >1.9 Ma with bedrock samples evidencing similar minimum apparent

Table 4Modelled exposure burial histories for samples with paired ²⁶Al/¹⁰Be analyses. Minimum histories assume zero erosion. EPP-05-CJF plots in above the erosion island. Erosion corrected histories are derived from forward modelling using parameters presented in Table 2.

Sample	Site	¹⁰ Be production rate	²⁶ Al production rate	²⁶ Al/ ¹⁰ Be production ratio (*) normalised	Minimum history	Erosion corrected history	1 Sigma
		$(atoms g^{-1} yr^{-1})$			(ka)	(ka)	(ka)
Sentinel Range							
B-LON-04- MJB	Long Gables	38.32	272.61	0.63	920	3050	1290
B-LON-10- MJB	Long Gables	48.39	343.12	0.45	3920	4820	310
LON-02-MJB	Long Gables	38.27	272.22	0.51	1300	3420	1270
LON-03-MJB	Long Gables	38.21	271.83	0.52	1240	3350	1290
LON-05-MJB	Long Gables	40.37	286.98	0.46	1820	3880	1020
LON-08-MJB	Long Gables	41.68	296.14	0.71	900	2560	1140
LON-12-MJB	Long Gables	35.73	254.39	0.46	1700	3770	1090
LON-15-MJB	Long Gables	34.17	243.44	0.30	2600	4720	1140
EPP-05-CJF	Mt Epperley	51.13	362.26	0.63	_	_	_
EPP-07-CJF	Mt Epperley	49.73	352.47	0.50	2280	3890	750
HUB01CJF	Mt Hubley	34.89	248.55	0.59	1140	3260	1340
HUB-02-CJF	Mt Hubley	34.58	246.36	0.46	1500	3600	1280
HUB-06-CJF	Mt Hubley	33.09	235.84	0.51	1260	3180	1500
HUB-08-CJF	Mt Hubley	32.48	231.56	0.40	1700	3870	1270
Heritage Range							
SOH-01-MJB	Sohalt Peaks	15.33	110.27	0.56	1200	3360	1210
SOH-04-CJF	Sohalt Peaks	11.35	81.96	0.42	2060	4110	940
SOH-04-MJB	Sohalt Peaks	13.13	94.67	0.73	460	750	190
SOH-05-CJF	Sohalt Peaks	11.32	81.74	0.65	520	1790	1370
WAIS Interior							
WLRD01	Mt Woollard	36.17	257.50	0.32	2560	4770	1110
WLRD04	Mt Woollard	35.06	249.44	0.76	740	2670	1370
MTJN01	Mt Johns	28.72	204.89	0.57	1180	3200	1320
MTJN03	Mt Johns	27.70	197.64	0.59	1100	3330	1320

exposure ages. Additionally, our analyses indicate that the trimline separates this landscape of glacial erosion from an older landscape where glacial erosion is absent. The low ²⁶Al/¹⁰Be ratios and very high nuclide concentrations indicate a very long exposure-burial history which, under a simplified assumption of cyclical exposure-burial, potentially pre-dates the Pliocene for at least some of our samples. A pre-Pliocene age for the glacial trimline would be consistent with evidence from marine cores for significant Antarctic cooling at ~14 Ma (Shevenell et al., 2004; Holbourn et al., 2014) which has been linked to expansion of the AIS (Halberstadt et al., 2021). Although the wider WAIS remained dynamic through the Pliocene (Naish et al., 2009) the preservation of very old landscapes at high elevations in the Ellsworth Mountains and elsewhere in West Antarctica (Sugden et al., 2017; Spector et al., 2020; this study) implies that at no time was the climate warm enough to produce significantly erosive warm-based glaciation in these locations.

6.2. Heritage Range

The Soholt and Edson sample sites share characteristics with sites in the southern Heritage Range where exposure age data has previously been reported (Hein et al., 2016; Sugden et al., 2017). All sites are

located below the trimline identified by Denton et al. (1992). They are characterised by extensive blue ice areas occurring on the lee side of the Heritage Range escarpment and associated with active blue ice moraines and, in both areas, nested suites of relict moraines below a distinct weathering limit (Bentley et al., 2010) are inferred to have been deposited by active blue ice moraines that were present on an elevated ice sheet surface (Fogwill et al., 2012; Hein et al., 2016). The sites' proximity, similarity in setting, and general consistency of results suggests that they share a glaciological history and that inferences made can be extrapolated between them.

Apparent ¹⁰Be exposure ages from the Soholt Peaks and Edson Hills do not exhibit a clear age-elevation trend albeit the youngest apparent age is also the lowest in elevation. The ages do however fall within the bounds of previously reported exposure age data from elsewhere in the Heritage Range (Bentley et al., 2010; Fogwill et al., 2012; Hein et al., 2016; Sugden et al., 2017). The samples presented here are located below the LGM weathering limit (Bentley et al., 2010) and are inferred to represent relict blue ice moraine deposits. The span of apparent exposure ages indicates preservation of some erratics under cold-based ice during successive glaciations, a pattern observed elsewhere in the Heritage Range (Hein et al., 2016).

Due to the propensity for preservation of material under cold based

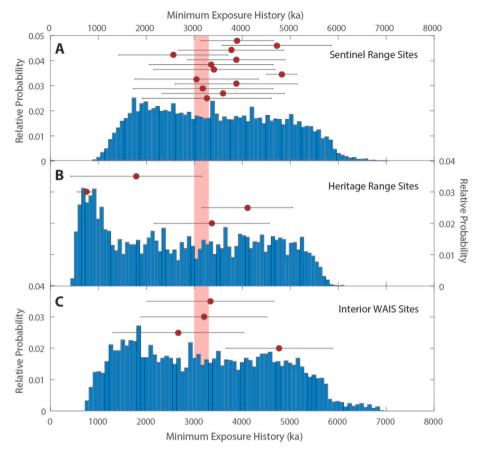


Fig. 9. Histograms of all minimum durations of modelled two-stage exposure-burial histories accounting for low erosion rates (cf. Marrero et al., 2018) for sites from A) Sentinel Range, B) Heritage Range and C) Interior WAIS sites. Individual sample means and associated one-sigma uncertainties are shown with red dots and associated error bars. Red shaded box delimits the mid-Pliocene warm period. (For interpretation of the references to colour in this figure legend, the reader is referred to the web version of this article.)

ice, once material is deposited as a relict moraine it is likely to remain in place. In this setting modelled exposure histories presented here suggest that the current ice flow configuration, which is required to produce blue ice moraines at the Soholt Peaks, has been established for at least 2.1 Ma, the longest modelled minimum history for a Soholt sample (SOH-04-CJF). Clasts on extant blue ice moraines in the Heritage Range have exposure histories <25 ka with emergent clasts having insignificant inventories of cosmogenic nuclides (Fogwill et al., 2012; Hein et al., 2016) supporting the inference that nuclide concentrations of relict blue ice material are predominantly the result of their exposure-burial history since initial deposition from englacial transport. Hein et al. (2016) argued that long exposure histories in the southern Heritage Range evidence a persistent location of the WAIS divide for at least 1.4 Ma. While we only present a single data point the oldest modelled history from Soholt Peaks potentially extend this inference to >2.1 Ma.

6.3. Interior WAIS sites

The data from the Pirrit Hills are the most limited, in terms of overall sample numbers and lack of paired nuclide measurements, of any site presented here. Consequently, inferences drawn from these samples are limited and inherently speculative. Apparent ¹⁰Be exposure ages from two glacially transported boulders in the Pirrit Hills are amongst the

oldest apparent exposure ages presented here (717 ka and 1.35 Ma). These ages are older than most boulder/clast ages in the larger dataset presented by Spector et al. (2019) however we note that they also report an exposure age of ~1 Ma from a large boulder. The samples were collected from ~300 m above present-day ice where blue ice moraines occur. Under the same model of deposition as in the Heritage Range (Section 4.2 and Hein et al., 2016) these ages suggest blue ice conditions, and hence the main WAIS divide location has persisted for at least 0.7-1.3 Ma (cf. Hein et al., 2016). An extension of the Ellsworth trimline, above which no glacial deposits are found, is reported from the Pirrit Hills (Spector et al., 2019, 2020). Bedrock samples from above this trimline exhibit no evidence for past ice cover and have very long exposure histories (9-12 Ma) implying constant sub-aerial exposure since the Miocene (Spector et al., 2020). The samples presented here are from glacial deposits and thus likely post-date formation of a higher erosional trimline. The apparent exposure ages of 0.7 and 1.3 Ma from our samples are consistent with a multi-million-year age (Sugden et al., 2017; Spector et al., 2020).

The high concentration and low 26 Al/ 10 Be ratio of WLRD01 indicates a very long exposure-burial history. This sample has a minimum two-stage history of \sim 2.6 Ma; accounting for erosion our two-stage model implies that this sample was first-exposed at least 4.8 \pm 1.1 Ma. Given the absence of higher topography in the area this estimate cannot be

Table 5Sensitivity of modelled minimum exposure histories to changes in assumed elevations of samples.

Sample	Site	Minimum history (ka)	500 m higher (ka)	500 m lower (ka)
Sentinel Range				
B-LON-04-MJB	Long Gables	920	Bedrock	Bedrock
B-LON-10-MJB	Long Gables	3920	Bedrock	Bedrock
LON-02-MJB	Long Gables	1300	1240	1420
LON-03-MJB	Long Gables	1240	1220	1340
LON-05-MJB	Long Gables	1820	1760	2060
LON-08-MJB	Long Gables	900	760	1140
LON-12-MJB	Long Gables	1700	1620	1940
LON-15-MJB	Long Gables	2600	2540	2840
EPP-07-CJF	Mt Epperley	2280	1960	3200
HUB01CJF	Mt Hubley	1140	1120	1200
HUB-02-CJF	Mt Hubley	1500	1420	1560
HUB-06-CJF	Mt Hubley	1260	1240	1200
HUB-08-CJF	Mt Hubley	1700	1720	1720
Heritage Range				
SOH-01-MJB	Sohalt Peaks	1200	1140	1380
SOH-04-CJF	Sohalt Peaks	2060	1920	2520
SOH-04-MJB	Sohalt Peaks	460	400	480
SOH-05-CJF	Sohalt Peaks	520	460	500
WAIS Interior				
WLRD01	Mt Woollard	2560	2520	2740
WLRD04	Mt Woollard	740	640	780
MTJN01	Mt Johns	1180	1080	1200
MTJN03	Mt Johns	1100	1160	1320

reduced by assuming that the sample was previously exposed at a higher elevation in the past. Similarly, any exposure at lower altitude or significant nuclide contribution from muons would result in our minimum history being an underestimate. It therefore seems reasonable to suggest that this sample records an exposure-burial history that is, at the very least, Pliocene in age (and potentially pre-dates it). One inference from this is that non-erosive, cold-based conditions have been prevalent at this site for a long time, with potential implications for the suitability of this site to test long term-ice sheet stability through sub-glacial drilling (cf. Spector et al., 2018).

Elsewhere in West Antarctica bedrock samples with long exposure histories suggest that ice at the WAIS divide experienced limited

expansion (<160–190 m higher than present) since the early Pliocene (Mukhopadhyay et al., 2012; Spector et al., 2020). Conversely, the samples from Mount Woollard and Mount Johns indicate significant periods of burial at elevations up to 267 m above present-day ice. Adapting our two-stage model to incorporate a period of exposure prior to sampling, the maximum modelled length of the current exposure period gives a maximum age of the most recent period of burial. We used the same model parameters as outlined in Table 2 but incorporated an additional period of exposure of 250 ka (guided by the apparent ¹⁰Be exposure ages), and 2 Ma (to test sensitivity). The results (Table 6) are consistent with a WAIS divide that has been up to ~200 m thicker during the Last Glacial Cycle, with burial potentially linked to LGM ice

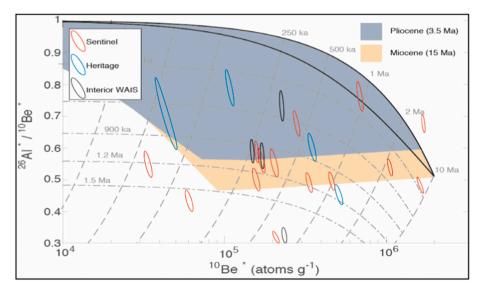


Fig. 10. Two-isotope (banana) plot of normalised (*) 26 Al/ 10 Be ratios and 10 Be concentrations for all samples with paired 26 Al/ 10 Be analyses. The shaded polygons delimit the parameter space (i.e. potential final ratios and concentrations) for cyclical exposure-burial over Pliocene (3.5 Ma) and Miocene (15 Ma) time periods.

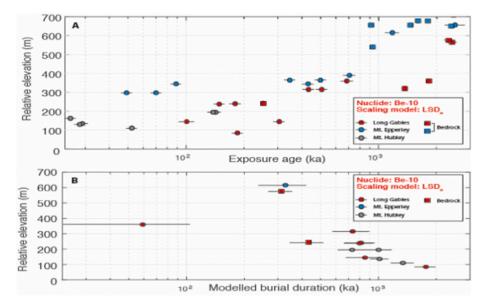


Fig. 11. A) Plot of exposure ages against elevation above present-day ice surface and B) plot of burial duration against elevation above present-day ice surface for samples from Sentinel Range. Note that the x-axes are logarithmic.

Table 6 Maximum modelled duration of current exposure period for samples from Mount Woollard and Mount Johns. Incorporating longer periods of exposure results in 10 Be concentrations and/or 26 Al/ 10 Be ratios inconsistent with measured values.

Sample	Site	Height above ice (m)	Maximum current exposure period (ka)
WLRD01	Mount Woollard	195	40
WLRD04	Mount Woollard	267	130
MTJN01	Mount Johns	100	60
MTJN03	Mount Johns	100	60

thickening. A thicker divide is supported by non-saturated in situ ¹⁴C ages from the Whitmore Mountains that require an ice surface \sim 190 m above present-day within the last 30 ka (Spector et al., 2019). However, low $^{26}\text{Al}/^{10}\text{Be}$ ratios evidence that our samples have experienced long (i. e., > > 100 ka) periods of burial throughout their history. This implies that ice was commonly thicker than present at these sites on the WAIS ice divide. This inference contrasts with, but does not necessarily contradict, a proposed scenario whereby ice at the divide has typically been thinner than present during the Pleistocene (Spector et al., 2020). It is interesting to note that transient model simulations of the WAIS over various timescales do not reproduce this thickening (Fig. 12). This may be explained by a variety of factors including model grid cell resolution, local ice accumulation, and over longer million-year timescales, the evolution of bed topography. Our data imply that existing simulations of the WAIS underestimate the amount of thickening over the Last Glacial Cycle at locations along the main ice divide.

7. Conclusions

Cosmogenic exposure age data from the Sentinel Range evidence a landscape below a distinct erosional trimline that has an exposure history that is millions of years old and potentially extends back to the Miocene. The formation of an erosional trimline, presumably by warmbased ice, during the Miocene is now evidenced from distal location

across the contemporary ice divide of West Antarctica implying that warm-based glaciation has been absent since this time. The overall distribution of exposure ages and burial signals shows an age-elevation trend that is consistent with a long-lived, cold-based ice sheet that has fluctuated in thickness but with an overall trajectory of declining surface elevation over time with respect to the Ellsworth Mountains. Samples from above the trimline have very high concentrations but plot slightly below isotopic equilibrium. Further data from the Heritage Range indicate that the present-day location of the ice divide is a persistent feature of the WAIS over million-year timescales as previously inferred.

Samples from nunataks in the interior of the WAIS have long exposure-burial histories that may also, in at least one instance, date to the Miocene. Additionally, these samples record complex exposure at elevations that lie above maximum modelled ice surface elevations over the last glacial cycle(s). While this mismatch may be explained by poorly constrained model boundary conditions it raises the interesting possibility that current simulations underestimate ice-sheet thickening in this part of West Antarctica during the Last Glacial Cycle and likely before.

Supplementary data to this article can be found online at https://doi.org/10.1016/j.geomorph.2025.109634.

CRediT authorship contribution statement

David Small: Writing - review & editing, Writing - original draft,

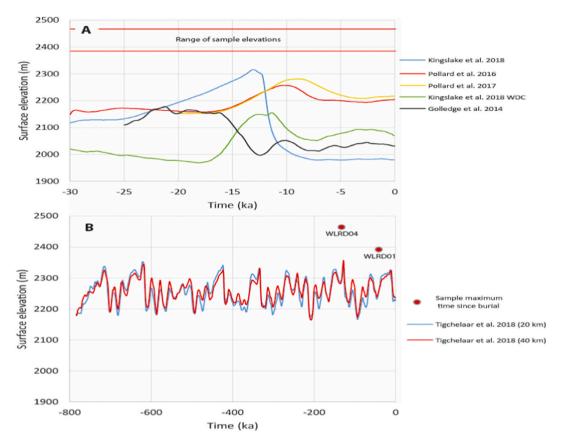


Fig. 12. Comparison of modelled ice sheet surface elevations at Mount Woollard and elevation of cosmogenic samples. A) Comparison of five ice sheet models spanning the last deglaciation (Golledge et al., 2014; Kingslake et al., 2018; Pollard et al., 2016, 2017). The red lines denote the elevation range of all samples from Mount Woollard. B) Comparison of ice sheet model spanning the last 800 ka (Tigchelaar et al., 2018) with differing cell size (20 km and 40 km). The red dots denote the maximum length of the most recent exposure period. Thus, burial must have occurred more recently. (For interpretation of the references to colour in this figure legend, the reader is referred to the web version of this article.)

Investigation, Formal analysis. **Michael J. Bentley:** Writing – review & editing, Writing – original draft, Methodology, Investigation, Funding acquisition, Data curation, Conceptualization. **Stewart P.H.T. Freeman:** Writing – review & editing, Writing – original draft, Investigation, Formal analysis, Data curation. **Angel Rodés:** Validation, Investigation, Formal analysis, Data curation. **Sheng Xu:** Validation, Investigation, Formal analysis, Data curation.

Declaration of competing interest

The authors declare the following financial interests/personal relationships which may be considered as potential competing interests: David Small reports financial support was provided by UK Research and Innovation Natural Environment Research Council. Michael Bentley reports financial support was provided by UK Research and Innovation Natural Environment Research Council. Michael Bentley reports financial support was provided by European Research Council. If there are other authors, they declare that they have no known competing financial interests or personal relationships that could have appeared to influence the work reported in this paper.

Acknowledgements

The samples reported here were collected under UK Natural Environment Research Council (NERC) grants to MB: NER/G/S/2003/00141 and NE/J005673/1. MB's involvement was supported by funding received from the European Research Council (ERC) under the European Union's Horizon 2020 research and innovation programme (grant agreement no. 885205, Project: 'INCISED'). Some samples were

analysed under NERC Cosmogenic isotope Facility allocation 9146.0414. DS was funded by Durham University Geography Department and by NERC Independent Research Fellowship NE/T011963/1. We are grateful to the pilots and support staff who facilitated sampling in some challenging areas, especially Rob Smith, Tom Marshall, Roger Stilwell, and Jack Beardsley, and to Elaine McDougall who assisted with the preparation of cosmogenic samples.

Data availability

Data will be made available on request.

References

Balco, G., Stone, J.O., Lifton, N.A., Dunai, T.J., 2008. A complete and easily accessible means of calculating surface exposure ages or erosion rates from 10Be and 26Al measurements. Quat. Geochronol. 3 (3), 174–195.

Balco, G., Stone, J.O., Sliwinski, M.G., Todd, C., 2014. Features of the glacial history of the Transantarctic Mountains inferred from cosmogenic 26 Al, 10 Be and 21 Ne concentrations in bedrock surfaces. Antarct. Sci. 26 (6), 708–723.

Balter-Kennedy, A., Bromley, G., Balco, G., Thomas, H., Jackson, M.S., 2020. A 14.5-million-year record of East Antarctic Ice Sheet fluctuations from the central Transantarctic Mountains, constrained with cosmogenic 3 He, 10 Be, 21 Ne, and 26 Al. Cryosphere 14 (8), 2647–2672.

Bentley, C.R., Crary, A.P., Ostenso, N.A., Thiel, E.C., 1960. Structure of West Antarctica. Science 131 (3394), 131–136.

Bentley, M.J., Fogwill, C.J., Le Brocq, A.M., Hubbard, A.L., Sugden, D.E., Dunai, T.J., Freeman, S.P., 2010. Deglacial history of the West Antarctic Ice Sheet in the Weddell Sea embayment: constraints on past ice volume change. Geology 38 (5), 411–414.

Bierman, P.R., Marsella, K.A., Patterson, C., Davis, P.T., Caffee, M., 1999. Mid-Pleistocene cosmogenic minimum-age limits for pre-Wisconsinan glacial surfaces in southwestern Minnesota and southern Baffin Island: a multiple nuclide approach. Geomorphology 27 (1–2), 25–39.

Bindschadler, R., Vornberger, P., Fleming, A., Fox, A., Mullins, J., Binnie, D., Paulsen, S. J., Granneman, B., Gorodetzky, D., 2008. The Landsat image mosaic of Antarctica. Remote Sens. Environ. 112 (12), 4214–4226.

- Bindschadler, R., Choi, H., Wichlacz, A., Bingham, B., Bohlander, J., Brunt, K., Corr, H., Drews, R., Fricker, H., Hall, M., Hindmarsh, R., 2011. Getting around Antarctica: new high-resolution mappings of the grounded and freely-floating boundaries of the Antarctic ice sheet created for the International Polar Year. Cryosphere 5, 569–588.
- Blasco, J., Tabone, I., Moreno-Parada, D., Robinson, A., Alvarez-Solas, J., Pattyn, F., Montoya, M., 2024. Antarctic tipping points triggered by the mid-Pliocene warm climate. Clim. Past 20 (9), 1919–1938.
- Borchers, B., Marrero, S., Balco, G., Caffee, M., Goehring, B., Lifton, N., Nishiizumi, K., Phillips, F., Schaefer, J., Stone, J., 2016. Geological calibration of spallation production rates in the CRONUS-Earth project. Quat. Geochronol. 31, 188–198.
- Briner, J.P., Lifton, N.A., Miller, G.H., Refsnider, K., Anderson, R., Finkel, R., 2014. Using in situ cosmogenic 10Be, 14C, and 26Al to decipher the history of polythermal ice sheets on Baffin Island, Arctic Canada. Quat. Geochronol. 19, 4–13.
- Casassa, G., Rivera, A., Acuña, C., Brecher, H., Lange, H., 2004. Elevation change and ice flow at Horseshoe Valley, Patriot Hills, West Antarctica. Ann. Glaciol. 39, 20–28.
- Child, D., Elliott, G., Mifsud, C., Smith, A.M., Fink, D., 2000. Sample processing for earth science studies at ANTARES. Nucl. Instrum. Methods Phys. Res., Sect. B 172 (1–4), 856–860.
- De Schepper, S., Gibbard, P.L., Salzmann, U., Ehlers, J., 2014. A global synthesis of the marine and terrestrial evidence for glaciation during the Pliocene Epoch. Earth Sci. Rev. 135, 83–102.
- Denton, G.H., Bockheim, J.G., Rutford, R.H., Andersen, B.G., 1992. Glacial history of the Ellsworth Mountains, West Antarctica. Geol. Soc. Am. Mem. 170, 403–432.
- Fabel, D., Ballantyne, C.K., Xu, S., 2012. Trimlines, blockfields, mountain-top erratics and the vertical dimensions of the last British–Irish Ice Sheet in NW Scotland. Quat. Sci. Rev. 55, 91–102.
- Fogwill, C.J., Hein, A.S., Bentley, M.J., Sugden, D.E., 2012. Do blue-ice moraines in the Heritage Range show the West Antarctic ice sheet survived the last interglacial? Palaeogeogr. Palaeoclimatol. Palaeoecol. 335, 61–70.
- Fretwell, P., Pritchard, H.D., Vaughan, D.G., Bamber, J.L., Barrand, N.E., Bell, R., Bianchi, C., Bingham, R.G., Blankenship, D.D., Casassa, G., Catania, G.A., 2013. Bedmap2: improved ice bed, surface and thickness datasets for Antarctica. Cryosphere 7, 375–393.
- Gasson, E., DeConto, R.M., Pollard, D., Levy, R.H., 2016. Dynamic Antarctic ice sheet during the early to mid-Miocene. Proc. Natl. Acad. Sci. 113 (13), 3459–3464.
- Golledge, N.R., Levy, R.H., McKay, R.M., Fogwill, C.J., White, D.A., Graham, A.G., Smith, J.A., Hillenbrand, C.D., Licht, K.J., Denton, G.H., Ackert Jr., R.P., 2013. Glaciology and geological signature of the Last Glacial Maximum Antarctic ice sheet. Quat. Sci. Rev. 78, 225–247.
- Golledge, N.R., Menviel, L., Carter, L., Fogwill, C.J., England, M.H., Cortese, G., Levy, R. H., 2014. Antarctic contribution to meltwater pulse 1A from reduced Southern Ocean overturning. Nat. Commun. 5, 5107.
- Grutzner, J., Rebesco, M.A., Cooper, A.K., Forsberg, C.F., Kryc, K.A., Wefer, G., 2003. Evidence for orbitally controlled size variations of the East Antarctic Ice Sheet during the late Miocene. Geology 31 (9), 777–780.
- Halberstadt, A.R.W., Chorley, H., Levy, R.H., Naish, T., DeConto, R.M., Gasson, E., Kowalewski, D.E., 2021. CO2 and tectonic controls on Antarctic climate and icesheet evolution in the mid-Miocene. Earth Planet. Sci. Lett. 564, 116908.
- Halberstadt, A.R.W., Gasson, E., Pollard, D., Marschalek, J., DeConto, R.M., 2024. Geologically constrained 2-million-year-long simulations of Antarctic Ice Sheet retreat and expansion through the Pliocene. Nat. Commun. 15 (1), 7014.
- Halsted, C.T., Bierman, P.R., Balco, G., 2021. Empirical evidence for latitude and altitude variation of the in situ cosmogenic 26Al/10Be production ratio. Geosciences 11 (10), 402.
- Haywood, A.M., Tindall, J.C., Burton, L.E., Chandler, M.A., Dolan, A.M., Dowsett, H.J., Feng, R., Fletcher, T.L., Foley, K.M., Hill, D.J., Hunter, S.J., 2024. Pliocene Model Intercomparison Project Phase 3 (PlioMIP3)–science plan and experimental design. Glob. Planet. Chang. 232, 104316.
- Hein, A.S., Woodward, J., Marrero, S.M., Dunning, S.A., Steig, E.J., Freeman, S.P., Stuart, F.M., Winter, K., Westoby, M.J., Sugden, D.E., 2016. Evidence for the stability of the West Antarctic Ice Sheet divide for 1.4 million years. Nat. Commun. 7, 10325.
- Holbourn, A., Kuhnt, W., Lyle, M., Schneider, L., Romero, O., Andersen, N., 2014. Middle Miocene climate cooling linked to intensification of eastern equatorial Pacific upwelling. Geology 42 (1), 19–22.
- Jones, R.S., Norton, K.P., Mackintosh, A.N., Anderson, J.T.H., Kubik, P., Vockenhuber, C., Wittmann, H., Fink, D., Wilson, G.S., Golledge, N.R., McKay, R., 2017. Cosmogenic nuclides constrain surface fluctuations of an East Antarctic outlet glacier since the Pliocene. Earth Planet. Sci. Lett. 480, 75–86.
- Jones, R.S., Small, D., Cahill, N., Bentley, M.J., Whitehouse, P.L., 2019. iceTEA: Tools for plotting and analysing cosmogenic-nuclide surface-exposure data from former ice margins. Quat. Geochronol. 51, 72–86.
- Kingslake, J., Scherer, R.P., Albrecht, T., Coenen, J., Powell, R.D., Reese, R., Stansell, N. D., Tulaczyk, S., Wearing, M.G., Whitehouse, P.L., 2018. Extensive retreat and readvance of the West Antarctic Ice Sheet during the Holocene. Nature 558 (7710), 420
- Kleman, J., Stroeven, A.P., 1997. Preglacial surface remnants and Quaternary glacial regimes in northwestern Sweden. Geomorphology 19 (1–2), 35–54.
- Kohl, C.P., Nishiizumi, K., 1992. Chemical isolation of quartz for measurement of in-situproduced cosmogenic nuclides. Geochim. Cosmochim. Acta 56 (9), 3583–3587.
- Levy, R., Harwood, D., Florindo, F., Sangiorgi, F., Tripati, R., Von Eynatten, H., Gasson, E., Kuhn, G., Tripati, A., DeConto, R., Fielding, C., 2016. Antarctic ice sheet

- sensitivity to atmospheric CO2 variations in the early to mid-Miocene. Proc. Natl. Acad. Sci. 113 (13), 3453–3458.
- Lifton, N., Sato, T., Dunai, T.J., 2014. Scaling in situ cosmogenic nuclide production rates using analytical approximations to atmospheric cosmic-ray fluxes. Earth Planet. Sci. Lett. 386, 149–160.
- Marrero, S.M., Phillips, F.M., Borchers, B., Lifton, N., Aumer, R., Balco, G., 2016. Cosmogenic nuclide systematics and the CRONUScalc program. Quat. Geochronol. 31, 160–187.
- Marrero, S.M., Hein, A.S., Naylor, M., Attal, M., Shanks, R., Winter, K., Woodward, J., Dunning, S., Westoby, M., Sugden, D., 2018. Controls on subaerial erosion rates in Antarctica. Earth Planet. Sci. Lett. 501, 56–66.
- Matsuoka, K., Skoglund, A., Roth, G., de Pomereu, J., Griffiths, H., Headland, R., Herried, B., Katsumata, K., Le Brocq, A., Licht, K., Morgan, F., 2021. Quantarctica, an integrated mapping environment for Antarctica, the Southern Ocean, and sub-Antarctic islands. Environ. Model Softw. 140, 105015.
- McCarroll, D., 2016. Trimline trauma: the wider implications of a paradigm shift in recognising and interpreting glacial limits. Scott. Geogr. J. 132, 130–139.
- Mukhopadhyay, S., Ackert Jr., R.P., Pope, A.E., Pollard, D., DeConto, R.M., 2012.
 Miocene to recent ice elevation variations from the interior of the West Antarctic ice sheet: constraints from geologic observations, cosmogenic nuclides and ice sheet modeling. Earth Planet. Sci. Lett. 337, 243–251.
- Naish, T., Powell, R., Levy, R., Wilson, G., Scherer, R., Talarico, F., Krissek, L., Niessen, F., Pompilio, M., Wilson, T., Carter, L., 2009. Obliquity-paced Pliocene West Antarctic ice sheet oscillations. Nature 458 (7236), 322.
- Napoleoni, F., Jamieson, S.S., Ross, N., Bentley, M.J., Rivera, A., Smith, A.M., Siegert, M. J., Paxman, G.J., Gacitúa, G., Uribe, J.A., Zamora, R., 2020. Subglacial lakes and hydrology across the Ellsworth subglacial highlands, West Antarctica. Cryosphere 14 (12). 4507–4524.
- Patterson, M.O., McKay, R., Naish, T., Escutia, C., Jimenez-Espejo, F.J., Raymo, M.E., Meyers, S.R., Tauxe, L., Brinkhuis, H., Expedition, I.O.D.P., Klaus, A., 2014. Orbital forcing of the East Antarctic ice sheet during the Pliocene and Early Pleistocene. Nat. Geosci. 7 (11), 841.
- Pollard, D., DeConto, R.M., 2009. Modelling West Antarctic ice sheet growth and collapse through the past five million years. Nature 458 (7236), 329.
- Pollard, D., Chang, W., Haran, M., Applegate, P., DeConto, R., 2016. Large Ensemble Modeling of the Last Deglacial Retreat of the West Antarctic Ice Sheet: Comparison of Simple and Advanced Statistical Techniques.
- Pollard, D., Gomez, N., Deconto, R.M., 2017. Variations of the Antarctic ice sheet in a coupled ice sheet-earth-sea level model: sensitivity to viscoelastic earth properties. J. Geophys. Res. Earth 122 (11), 2124–2138.
- Ross, N., Jordan, T.A., Bingham, R.G., Corr, H.F., Ferraccioli, F., Le Brocq, A., Rippin, D. M., Wright, A.P., Siegert, M.J., 2014. The Ellsworth subglacial highlands: inception and retreat of the West Antarctic Ice Sheet. Bulletin 126 (1–2), 3–15.
- Shevenell, A.E., Kennett, J.P., Lea, D.W., 2004. Middle Miocene southern ocean cooling and Antarctic cryosphere expansion. Science 305 (5691), 1766–1770.
- Siegert, M.J., Hindmarsh, R., Corr, H., Smith, A., Woodward, J., King, E.C., Payne, A.J., Joughin, I., 2004. Subglacial Lake Ellsworth: a candidate for in situ exploration in West Antarctica. Geophys. Res. Lett. 31 (23), L23403.
- Small, D., Bentley, M.J., Evans, D.J., Hein, A.S., Freeman, S.P., 2021. Ice-free valleys in the Neptune Range of the Pensacola Mountains, Antarctica: glacial geomorphology, geochronology and potential as palaeoenvironmental archives. Antarct. Sci. 33 (4), 428–455.
- Spector, P., Stone, J., Pollard, D., Hillebrand, T., Lewis, C., Gombiner, J., 2018. West Antarctic sites for subglacial drilling to test for past ice-sheet collapse. Cryosphere 12 (8), 2741–2757.
- Spector, P., Stone, J., Goehring, B., 2019. Thickness of the divide and flank of the West Antarctic Ice Sheet through the last deglaciation. Cryosphere. https://doi.org/ 10.5195/tc-2019-115.
- Spector, P., Stone, J., Balco, G., Hillebrand, T., Thompson, M., Black, T., 2020. Miocene to Pleistocene history of West Antarctica inferred from nunatak geomorphology and cosmogenic-nuclide measurements on bedrock surfaces. Am. J. Sci. 320, 637–676.
- Sugden, D.E., Hein, A.S., Woodward, J., Marrero, S.M., Rodés, Á., Dunning, S.A., Stuart, F.M., Freeman, S.P., Winter, K., Westoby, M.J., 2017. The million-year evolution of the glacial trimline in the southernmost Ellsworth Mountains, Antarctica. Earth Planet. Sci. Lett. 469, 42–52.
- Tigchelaar, M., Timmermann, A., Pollard, D., Friedrich, T., Heinemann, M., 2018. Local insolation changes enhance Antarctic interglacials: Insights from an 800,000-year ice sheet simulation with transient climate forcing. Earth Planet. Sci. Lett. 495, 69–78.
- Warny, S., Askin, R.A., Hannah, M.J., Mohr, B.A., Raine, J.I., Harwood, D.M., Florindo, F., SMS Science Team, 2009. Palynomorphs from a sediment core reveal a sudden remarkably warm Antarctica during the middle Miocene. Geology 37 (10), 955–958.
- Webers, G.F., Sporli, K.B., 1983. Palaeontological and Stratigraphic Investigations in the Ellsworth Mountains, West Antarctica. Antarctic Earth Science. Australian Academy of Science, Canberra, pp. 261–264.
- Westoby, M., Dunning, S., Woodward, J., Hein, A., Marrero, S., Winter, K., Sugden, D., 2016. Interannual surface evolution of an Antarctic blue-ice moraine using multitemporal DEMs. Earth Surf. Dyn. 4 (2), 515–529.
- Woodward, J., Hein, A.S., Winter, K., Westoby, M.J., Marrero, S.M., Dunning, S.A., Lim, M., Rivera, A., Sugden, D.E., 2022. Blue-ice moraines formation in the Heritage Range, West Antarctica: Implications for ice sheet history and climate reconstruction. Quaternary Science Advances 6 p.100051.
- Xu, S., Dougans, A.B., Freeman, S.P., Schnabel, C., Wilcken, K.M., 2010. Improved 10Be and 26Al-AMS with a 5 MV spectrometer. Nucl. Instrum. Methods Phys. Res., Sect. B 268 (7–8), 736–738.